Qualitative and Quantitative Analyses of Hazardous Compounds from NTPC Rihand, India

Pramod Kumar
Environmental Monitoring Laboratory, Environmental Toxicology Group, CSIR- Indian Institute of Toxicology Research (CSIR-IITR)

Manvendra Verma
Department of Civil Engineering, GLA University

Pramod Kumar
Department of Environmental Science, Deshbandhu College, University of Delhi

Pokhraj Sahu
Division of Environment Science, School of Basic Sciences, Babu Banarasi Das University

他

https://doi.org/10.5109/7388837

出版情報：Evergreen. 12 (3), pp.1402-1417, 2025-09. 九州大学グリーンテクノロジー研究教育センター
バージョン：

Qualitative and Quantitative Analyses of Hazardous Compounds from NTPC Rihand, India

Pramod Kumar[1, 2], Manvendra Verma[3,*], Pramod Kumar[4], Pokhraj Sahu[5], Shailendra Kumar Yadav[6], Ganesh Chandra Kisku[1,2]

[1]Environmental Monitoring Laboratory, Environmental Toxicology Group, CSIR- Indian Institute of Toxicology Research (CSIR-IITR), Vishvigyan Bhawan, 31, Mahatma Gandhi Marg, Lucknow-226001, Uttar Pradesh, India
[2]Academy of Scientific and Innovative Research (AcSIR), Ghaziabad-201002, India.
[3]Department of Civil Engineering, GLA University, Mathura-281406, Uttar Pradesh, India
[4]Department of Environmental Science, Deshbandhu College, University of Delhi, New Delhi-110019, India
[5]Division of Environment Science, School of Basic Sciences, Babu Banarasi Das University, Lucknow-226028, Uttar Pradesh, India
[6]Department of Environmental Science, Babasaheb Bhimrao Ambedkar University, Lucknow-226025, Uttar Pradesh, India

*Author to whom correspondence should be addressed:
E-mail: mv075415@gmail.com

(Received September 03, 2024; Revised June 13, 2025; Accepted August 15, 2025)

Abstract: Multiple hazardous compounds, including gases, heavy metals (HMs), and polycyclic aromatic hydrocarbons (PAHs), are released during coal combustion in coal-fired power plants (C-FPPs). Pollutants impact environment and human health negatively. To understand hazardous pollutants, this study collected samples from a coal-fired thermal power station. Scanning electron microscopy (SEM) and Fourier-transform infrared spectroscopy (FTIR) were used to characterize the coal and its residues. Ten HMs (Cd, Co, Cr, Cu, Ni, Pb, Zn, As, Se, and Hg) were identified and measured. The highest concentration of Pb (90.41±6.41 mg/kg) was measured in coal, while 201.69±35.69 mg/kg and 178.80±73.22 mg/kg were noted for coal-fly ash (CFA) and bottom ash (BA) samples. PAHs contents ∑16PAHs were highest for Fluorene + Acenaphthene (33.81±2.56 mg/kg). Post-hoc test showed all analyzed HMs except Cu were significantly transferred from coal to CFA, whereas only Co, Cr, and Zn were significantly transferred to BA. ∑16PAHs were significantly transferred from CFA except for fluorene + acenaphthene and anthracene, while all PAHs were significantly transferred to BA except anthracene. Analysis of variance (ANOVA) revealed a statistically significant effect of $p < 0.05$. High quantities of HMs and PAHs in coal, CFA, and BA samples could cause air, soil, and water pollution.

Keywords: Coal-fired power plant; Coal Fly ash; Heavy metals; Polycyclic aromatic compounds; Toxic hazards

1. Introduction

Coal is one of the cheapest and most widely available energy sources on Earth. Since industrial revolution, coal has significantly raised world economy and played a key factor in the production of electricity worldwide, including in India. Worldwide contribution of coal in the energy sector is high (37%), including India, with 50.7% in 2023 and 55.4% in 2020-2021, and is expected to retain its position as the single largest electricity source until 2040, worldwide[1,2)]. India's energy consumption will reach around 800,000 MW by 2030. The negative consequences of electricity generation from C-FPPs are geographical and environmental degradation, in terms of air, water, and soil pollution and ecosystem imbalance[3,4)].

Apart from the environmental challenge, emissions from C-FPP also affect human health from local to global. Coal fly ash (CFA) is a multifaceted byproduct of pulverized coal combustion in thermal power plants. Due to its complexity, roughly 316 minerals have been detected

Cite: P. Kumar et al., "Qualitative and Quantitative Analyses of Hazardous Compounds from NTPC Rihand, India". Evergreen, 12 (03) 1402-1417 (2025). https://doi.org/10.5109/7388837.

separately, while 188 minerals have been identified in groupings in diverse CFA samples from across the world. CFA possesses unique properties such as high volume, negative surface charge, porous structure, unburned carbon, cenospheres, and chemical reactivity, making it effective for adsorbing hazardous pollutants[5,6].

Coal burning causes environmental challenges worldwide, including acid rain, fine particle discharge, and greenhouse gas emissions. More than 85 thermal power plants in India generate approximately 120 MT of CFA annually, with predictions of 442 MT/year by 2035. The C-FPP, is a significant source of ambient heavy metals. CFA is often regarded as an environmental issue owing to the presence of potentially toxic elements such as mercury (Hg), lead (Pb), nickel (Ni), zinc (Zn), manganese (Mn), arsenic (As), and many others.

Mineralogy, particle size, and combustion temperature affect heavy metals (HMs) in CFA. Fine fly ash particle, polycyclic aromatic hydrocarbons (PAHs), volatile organic compounds (VOCs), HMs, and 84 of 187 hazardous air pollutants (HAPs) are discharged from C-TPPs[8,9]). CFA and coal dust create particulate matter (PM), which can cause lung cancer, chronic obstructive pulmonary disease (COPD), skin impairment, and other forms of cancer. The International Agency for Research on Cancer (IARC) classifies certain HM as category 1 carcinogens, including arsenic (As), cadmium (Cd), chromium (Cr), and nickel (Ni), while lead (Pb) is a category 2A carcinogen[10,11]. People living close to C-FPP, must be prevented from CFA-mediated hazards throughout the atmosphere.

Lowering the massive volumes of NOx, SO_2, CO_2, and CO generated during coal mining and burning has received considerable attention. Various HM, including As, Co, Cd, Ni, Cu, Cr, Mn, and Pb, were found entrapped in particulate matter (PM) by ambient CFA; their presence must be reduced for environmental sustainability.

Various forms of cancer, birth deformities, organ dysfunction, nervous system disorders, skin lesions and immune system impairment may result from HMs. The HMs' toxicity mechanism involves ROS production, enzyme inactivation, and antioxidant defense suppression[12,13]. Toxicities may manifest in a variety of ways through distinct modes of exposure, such as ingestion, inhalation, and dermal. HM-mediated harmful pathways may enable us to comprehend its effects on body organs, which lead us to manage and combat negative impacts on humans. Chemicals in the environment, such as Cr and Cd, may cause genetic instability[14,15]. Mercury affects the central nervous system (CNS), causing memory loss, tremors, and cognitive impairment, and impacts on fetal development in pregnant women. Lead is associated with neurological damage in newborns and young children. In addition to a negative impact on cognitive development as well as cardiovascular and renal health. Exposure to arsenic can lead to lung damage, skin lesions, and various types of cancer, including lung, skin, bladder, and liver cancer in addition to respiratory and cardiovascular illnesses. Chronic obstructive pulmonary disease (COPD) and lung cancer, kidney injury, osteoporosis, and cardiovascular issues are the results of cadmium toxicity[16,17]. Chromium exposure is associated with asthma and lung cancer, as well as skin allergies and dermatitis. Scientists hypothesized that the abnormalities caused by the two metals' induction of oxidative stress and impairment of DNA may lead to carcinogenicity.

The Indian C-FPP emitted more pollution per megawatt of electricity production compared to global standards and developed nations such as Australia, China, and the European Union. This can be attributed to several factors: the coal contains high ash content of approximately 34% and low calorific value from low carbon content; most Indian power plants operate within lower efficiency categories of the subcritical (34.3%) and supercritical (38.5%); there is inadequate pollution mitigation technology; and there are some high concentrations of toxic elements like mercury. Sampling, qualitative, and quantitative screenings of CFA in the environment are needed to Figure out how much HM is in the air environment and how much of a health risk it poses[18,19]. Nonetheless, each C-FPP discharges a different quantity of CFA into the atmosphere. In this work, qualitative and quantitative tests of metal pollutants were carried out on coal, CFA and BA from the NTPC Rihand super thermal power plant in order to get a comprehension of the chemical characteristics of coal-based pollutants[20,21].

2. Materials and methods

2.1. Brief description of the study area

Singrauli is located in the eastern region of Madhya Pradesh and the southern part of Uttar Pradesh's Sonbhadra district. Singrauli, known as the “Energy Capital of India” incorporates natural resources such as coal and minerals. Singrauli is 5672 km^2 and located at 23 49' N, 24 42' N, 81 18' E, 82 48' E, and 609 meters above sea level. January temperatures range from 5.4°C to 21.6°C, while summer temperatures reach 45.3°C in May and 31.9°C in June. Annual rainfall averages 1100 millimeters between July and September. Upwards of 11,000 MW to 33,000 MW of power might be generated in the area. With a Comprehensive Environmental Pollution Index (CEPI) score of 83.24, Singrauli is one of the most polluted industrial cluster in India out of a total of 88 industrial clusters (CPCB, 2018)[22,23].

2.2. Collection of coal, CFA, and BA samples

Coal: For this study, samples of coal, CFA, and BA were taken from M/s Rihand Super thermal power plant in Sonbhadra, Uttar Pradesh, India. The coal sample was

Cite: P. Kumar et al., "Qualitative and Quantitative Analyses of Hazardous Compounds from NTPC Rihand, India". Evergreen, 12 (03) 1402-1417 (2025). https://doi.org/10.5109/7388837.

collected in a plastic bag from the coal feeding location before being used as boiler fuel. After collection, it was wrapped and stored in dark, dry conditions at room temperature. The sample was placed in a desiccator for 24 hours before HMs and PAHs content analyses.[24,25)]

Coal fly ash: CFA was collected near the electrostatic precipitator (ESP) hopper in plastic bags, sealed onsite, and stored in a dark, dry environment at room temperature until analyses[26)].

Bottom ash: Bottom ash (BA) is a mixture of CFA and coal after incomplete burning, making it heavier than CFA. BA comprises 20% of a power plant's total CFA output. BA was collected from the boiler unit, washed with water, dried and stored at room temperature in dark conditions[27)].

Table 1: Concentration (mg/kg) of heavy metals in coal, CFA and BA

Heavy metal	Coal	CFA	BA
As	0.37±0.24	3.44±1.10	0.37±30
Cd	0.33±0.58	2.69±0.62	1.33±0.58
Co	6.09±1.84	29.59±8.48	20.08±5.67
Cr	34.11±2.07	85.21±7.50	83.03±25.81
Cu	36.09±35.71	36.54±4.29	27.24±5.93
Hg	0.14±0.17	0.79±0.35	0.59±0.20
Ni	25.68±18.52	53.21±4.74	45.75±11.86
Pb	90.41±6.41	201.69±35.69	178.80±73.22
Se	0.09±0.05	0.63±0.29	0.24±0.10
Zn	25.71±8.57	109.88±5.89	77.47±34.79

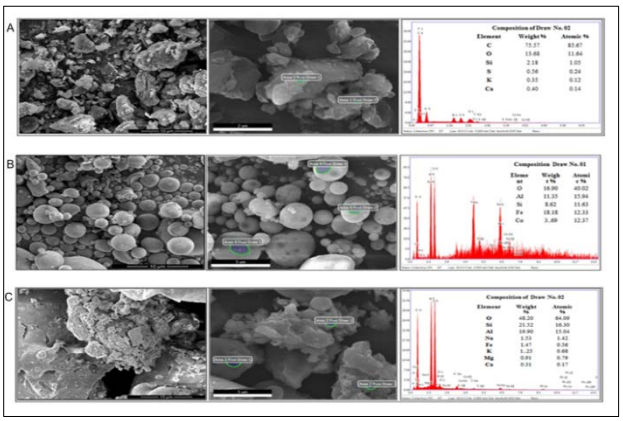

Fig. 1: Photomicrographs of SEM with EDX spectra. A: SEM-EDX analysis of coal sample (Left: SEM image, middle: EDX, Right: EDX spectra graph). B: SEM-EDX analysis of CFA sample (Left: SEM image, middle: EDX, Right: EDX spectra graph). C: SEM-EDX analysis of BA sample (Left: SEM image, middle: EDX, Right: EDX spectra graph).

2.3. Morphological and chemical composition analyses of coal and CFA with Scanning Electron Microscopy (SEM) with Energy Dispersive X-Ray Analysis (EDX)

Energy-dispersive X-ray spectroscopy (EDX) determined elemental compositions of coal, coal fly ash (CFA), and bottom ash (BA) samples. Although scanning electron microscopy (SEM) (ZEISS EVO, Germany) provided surface topography and elemental mapping, it could not detect organic constituents or amorphous iron oxides. Selected metals (Zn, Pb, Cr, Cu, and V) were analyzed due to measurable abundance. Samples were sieved, desiccated for 24 hours, and mounted on metallic stubs with platinum coating for enhanced resolution. EDX analysis relied on characteristic X-ray emissions from electron interactions at 20 kV for elemental identification[28–30)].

2.4. Fourier-transform infrared spectroscopy (FTIR) analyses

Fourier-transform infrared (FTIR) spectroscopy has been extensively employed to characterize the chemical composition and functional groups in coal minerals. These investigations primarily concentrated on identifying inorganic mineral phases (e.g., quartz, clays, carbonates) and organic functional groups to evaluate coal rank, maturity, and reactivity. It detects several different functional structures that are present in the specimens. Infrared light is used in the FTIR analysis method to scan materials and determine the chemical qualities they contain. The principle involves raising molecular vibration frequency by light energy absorption to excite bonds. FTIR analyzes chemical composition and physical condition of samples by recording spectra between 4000 and 400 cm-1 (wavelengths 2.5 to 25 µm) to identify materials. Further analysis determined functional groups in samples.

2.5. Heavy metal estimation

Approximately 2g of dried material was accurately weighed into a sealed Teflon vial containing a tri-acid digestion solution. (HNO_3, $HClO_4$, and HF 5:1:1 v/v). The mixture left overnight to facilitate the estimation of heavy metals. The digestion process was conducted at 105 °C until the solution became transparent, after which it was filtered and diluted to a final volume of 20 ml using 0.1 N HNO_3. The concentrations of heavy metals were determined using an Atomic Absorption Spectrophotometer (AAS, Model GBC Avanta Sigma). Specifically, the elements Cd, Co, Cr, Cu, Ni, Pb, and Zn were analyzed via AAS, whereas As, Se, and Hg were quantified using Atomic Fluorescence Spectroscopy (AFS). For the AFS analysis, 2g of moisture-free samples were digested overnight with H_2SO_4. Subsequently, 6% $KMNO_4$ was added under ice in darkness for 15-20 minutes until a pink color was observed, followed by the

addition of 20% hydroxylamine hydrochloride until the solution became colorless. Samples were diluted to 20 ml, filtered, and analyzed in triplicate with values mean ± SD (n=3)[31,32].

2.6. Polycyclic aromatic hydrocarbon (PAH) quantification by extraction method with Soxhlet and HPLC

Coal, CFA and BA samples (5.0 g each) were Soxhlet extracted for 16 hours with 150 mL of dichloromethane (DCM) to PAH investigation. Post-extraction, the samples were concentrated using a rotary evaporator at a temperature range of 22–25°C, following de-moisturization with anhydrous granular sodium sulfate. The solvent was then transitioned to acetonitrile, diluted to a volume of 2 mL, and filtered into amber gas chromatography (GC) vials using a polytetrafluoroethylene (PTFE) membrane filter with a pore size of 0.22μm (Millipore). The samples were stored at 4°C and subjected to analysis within 15 days using Ultra High-Performance Liquid Chromatography (UHPLC) with photodiode array detector (Nexara SR, Shimadzu Corp.) using a modified reported procedure. Chromatographic separation used an analytical column (Zorbax, Extend - C18 (2.1 × 150 mm), 1.8μm particle size). Acetonitrile: water mixture (80:20, v/v) served as mobile phase (0.4 ml/min) at ambient temperature. A 2μL sample was injected for isocratic elution with 13 min run time. Data was processed using LC solution software for peak integration and quantification[33–35].

2.7. Quality assurance and quality control

Each sample was treated carefully to ensure flawless processing. Reproducible findings were ensured by following quality assurance processes and precautions. The entire experiment utilized deionized water. Prior to use, glassware was immersed in chromic acid overnight, then thoroughly cleaned and dried. Throughout the experiment, only chemicals of the highest analytical grade were employed.

2.8. Statistical analysis

Data analysis was conducted using SPSS software (Windows Version 22), employing one-way analysis of variance (ANOVA), LSD post-hoc tests, hierarchical cluster analysis (HCA), Pearson correlation analysis, and descriptive statistics (mean and SEM). The dataset was subjected to ANOVA to compare mean and relative differences. Specifically, one-way ANOVA was performed on the contents of heavy metals (HMs) and polycyclic aromatic hydrocarbons (PAHs) in coal, coal fly ash (CFA), and bottom ash (BA), followed by an LSD post-hoc multi-comparison test. The Ward linkage method was utilized for the linkage algorithm, and a rescaled distance cluster was employed to evaluate distance. The correlation matrix, a statistical technique, was used to determine the significance of relationships between two datasets at the 0.01 and 0.05 levels. The datasets of PAHs and HMs in coal, CFA, and BA were analyzed to examine these correlation [35–38].

3. Results and discussion

3.1. Morphological and chemical composition of coal and CFA with Scanning Electron Microscopy (SEM) with Energy Dispersive X-Ray Analysis (EDX)

Scanning electron microscopy (SEM) photomicrographs of coal, coal fly ash (CFA), and bottom ash (BA) samples (Figure 1 A–C) elucidated three-dimensional morphological characteristics at near-atomic resolution. Coal particles are characterized by irregular shapes and coarse textures, whereas CFA comprises fine, spherical, and occasionally agglomerated particles. In contrast, BA exhibits distinct morphological differences, lacking the spherical structures observed in CFA. Photomicrographs of coal, CFA, and BA with EDX spectra are depicted in subsequent Figures. The SEM microphotographs clearly reveal the particle size and chemistry of coal mineralization. SEM-EDX analysis confirmed the presence of both amorphous and crystalline phases in CFA. The coal sample predominantly contained C (75.57%), O, Si, S, K, and Ca (0.40%), whereas CFA demonstrated elevated concentrations of O (16.90%), Al (11.35%), Si (8.62%), Fe (18.18%), and Co (3.69%). BA exhibited higher proportions of O (48.20%), Si (21.52%), Al (19.90%), and trace amounts of Na, Fe, K, Mg, and Ca. Previous studies (Essex et al., 2017; Saikia et al., 2015) have similarly utilized SEM-EDX for the characterization of coal and CFA, thereby validating its efficacy in particle morphology and elemental analysis[24,39,40].

3.2. Fourier-transform infrared spectroscopy (FTIR) analyses

Fourier transform infrared (FT-IR) spectroscopy characterizes coal and isolates functional groups through infrared measurements. Aliphatic C-O-C stretching, -OH and -NH stretching vibrations, and HCC rocking have all been detected using FT-IR analysis, along with aliphatic -CH, -CH2, and -CH3 groups. Two-stage leaching with HNO3 and HF may have considerably reduced the ash content and mineral concentrations, especially those of Al, Si, and Ca. FTIR study reveals the presence of aliphatic -CH, -CH2, and -CH3 groups, aliphatic C-O-C stretching associated with -OH and -NH stretching vibrations, and HCC rocking in samples. FTIR spectra of the sample are portrayed in Figure 2 (A-C). FTIR characterization of coal minerals has been reported by different researchers in previous decades for the characterization of chemical

properties of coals. In contrast, to existing studies, the present study reveals a higher peak (functional group detection) in coal samples while comparatively low in coal-CFA and BA samples[41,42].

3.3. Heavy metal estimation

The concentrations of HMs in coal, CFA, and BA were analyzed to assess their comparative distribution. Two analytical methods were employed to detect ten HMs (Cd, Co, Cr, Cu, Ni, Pb, Zn, As, Se, and Hg). In contrast to the available study, in HMs were estimated from sample (n=3). The results revealed, CFA showed higher HM concentrations than BA, suggesting that combustion processes may lead to the enrichment of certain metals in finer particulate fractions. Among the analyzed HMs, Pb was found to be the most prevalent across all sample types, with the highest concentrations observed in coal (90.41 ± 6.41 mg/kg), CFA (201.69 ± 35.69 mg/kg), and BA (178.78 ± 73.22 mg/kg) (Figure 3). This trend aligns with previous studies showing elevated Pb levels in coal combustion byproducts, likely due to its volatility and tendency to concentrate in the fly ash. In contrast, Se displayed the lowest concentrations, with values of 0.09 ± 0.05 mg/kg in coal, 0.63 ± 0.29 mg/kg in CFA, and 0.24 ± 0.10 mg/kg in BA (Table 1).

The increased concentration of HMs in CFA compared to that in BA can be attributed to the volatilization of metallic elements during combustion, followed by their condensation onto finer particulate matter. Although this study quantified HM concentrations for comparative purposes, it did not evaluate potential health or environmental risks; as such an assessment would require further investigation of metal speciation and bioavailability. These findings are consistent with previous studies on heavy metal enrichment in CFA, highlighting the importance of effective management strategies for coal combustion residues to mitigate ecological hazards. Variations in HM concentrations can be attributed to multiple factors, including the geochemical composition of the parent coal material, combustion conditions, and operational parameters of the power plant. Therefore, site-specific characterization is crucial for accurate environmental risk assessment and regulatory decision making.

3.4. PAH quantification by extraction method with Soxhlet extractor and HPLC

PAHs are persistent environmental pollutants predominantly generated through the incomplete combustion of organic materials, such as coal. Structurally, PAHs consist of two or more fused benzene rings, along with reactive derivatives such as DNA-binding adducts and epoxides. These compounds exhibit carcinogenic, teratogenic, and mutagenic properties by inducing DNA damage and promoting genomic instability in critical regulatory regions. In this study, 16 priority PAHs were quantified in coal, CFA, and BA samples, with concentrations ranging from 0.001 ± 0.01 to 56.85 ± 11.86 mg/kg (Table 2, Figure 4). Notably, co-elution challenges hindered the individual quantification of certain PAH pairs Fluorene + Acenaphthene, Benz(a)anthracene + Chrysene, and Indeno[1,2,3-cd] pyrene + Benz (g,h,i)perylene due to their overlapping chromatographic peaks. Among the analyzed PAHs, the combined concentration of Fluorene and Acenaphthene (33.81 ± 2.56 mg/kg) was the highest, indicating their significant contribution to the overall PAH burden in the studied samples. The persistence nature of PAHs raises concerns about their potential for environmental contamination and bioaccumulation. Strategies to mitigate PAHs release from C-FPP implementing advanced treatment technologies, enhancing disposal methods, and alternative sustainable energy sources. Monitoring and risk assessment programs are essential to evaluate PAHs impacts from coal ash on soil, water, air quality, and local biota.

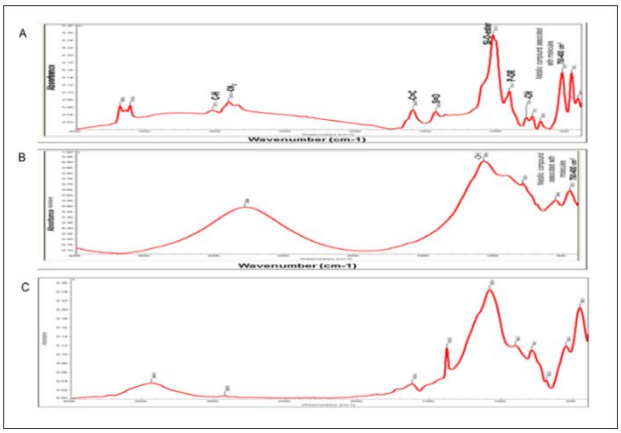

Fig. 2: FTIR spectra plot of samples. A: FTIR spectra of coal sample. B: FTIR spectra of coal-fly ash sample: FTIR spectra of bottom ash sample

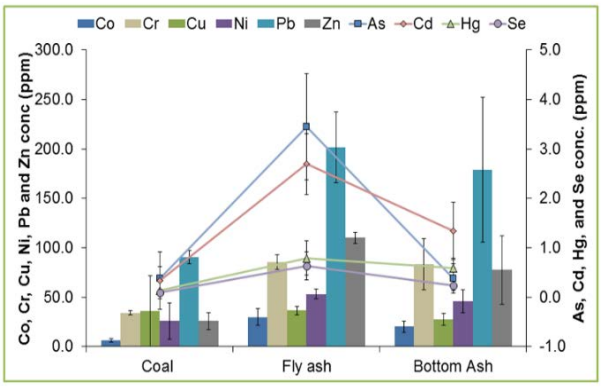

Fig. 3: Comparative metal quantification plot depicting ten quantified metals

Table 2: Concentration (mg/kg) of PAHs in coal, CFA, and BA

PAHs	Coal	CFA	BA
Naphthalene	5.65±0.25	0.48±0.17	0.34±0.10
Acenaphthylene	3.36±0.48	0.22±0.04	0.10.07
Fluorene + Acenaphthene	33.81±2.56	34.73±2.52	56.85±11.86
Phenanthrene	2.12±0.08	0.07±0.03	0.04±0.01
Anthracene	0.04±0.02	0.01±0.01	0.05±0.04
Fluoranthene	2.08±0.16	0.08±0.03	0.22±0.06
Pyrene	2.25±0.10	0.06±0.02	0.28±0.38
Benz(a)anthracene + Chrysene	2.43±0.22	0.09±0.01	0.05±0.03
Benz(k)fluorenthene	7.08±0.20	0.14±0.03	0.18±0.03
Benz(b)fluorenthene	2.54±0.29	Not Detected	Not Detected
Benz(a)pyrene	0.01±0.02	0.07±0.02	0.02±0.01
Dibenz(a,h)anthracene	0.77±0.32	0.06±0.10	Not Detected
Indeno[1,2,3-d]pyrene + Benz(g,h,i)perylene	7.17±0.24	0.10±0.09	0.46±0.11

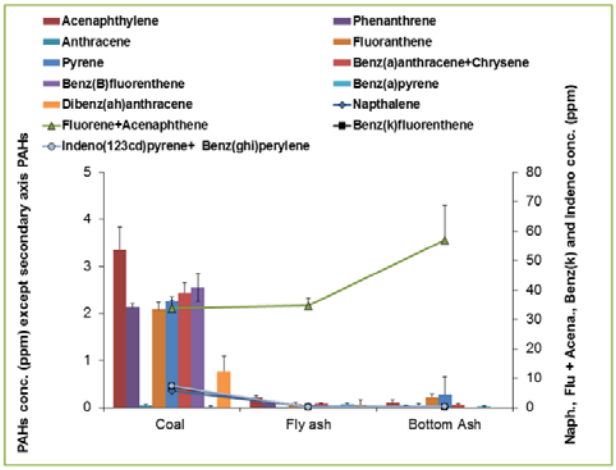

Fig. 4: Comparative Polycyclic Aromatic Compounds (PAHs) quantification plot depicting Σ16PAHs

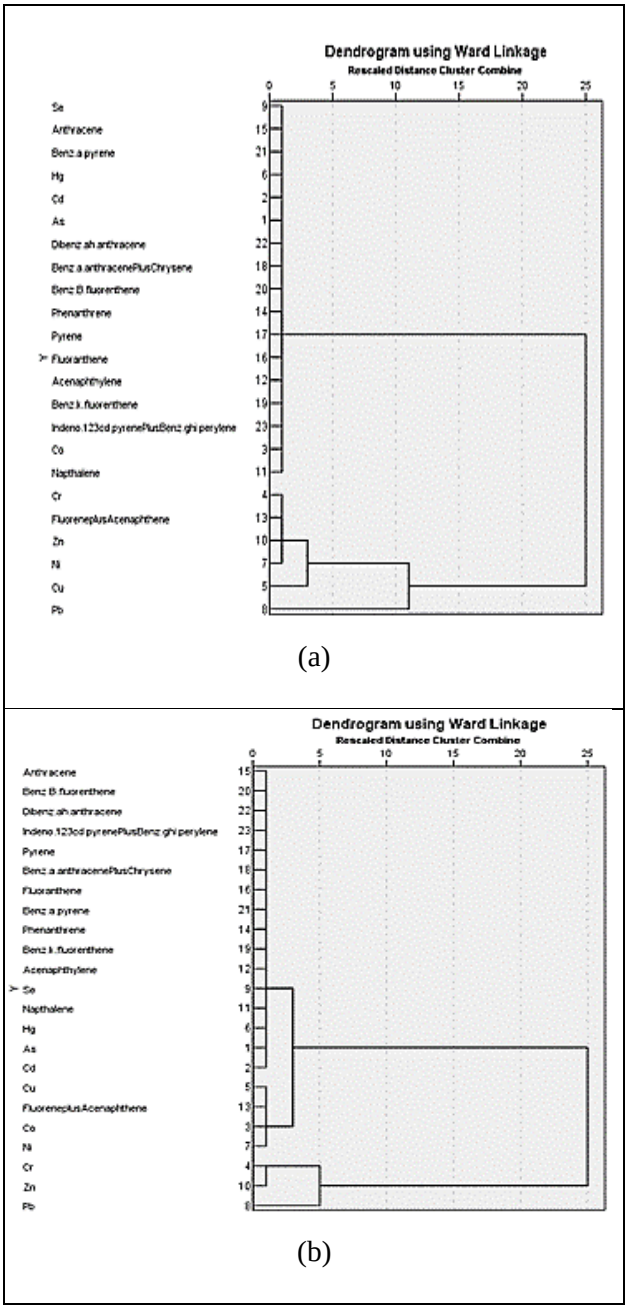

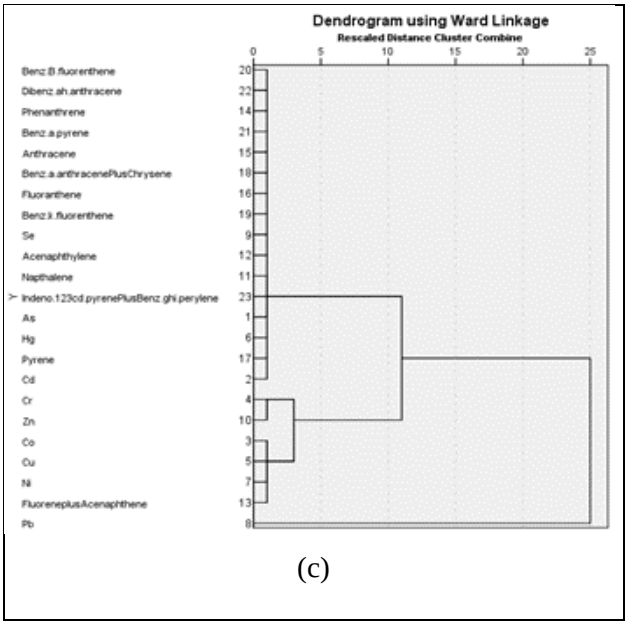

(c)

Fig. 5: Dendrogram of cluster analysis for HMs and PAHs in coal (a), CFA (b), and BA (c) samples

3.5. Statistical analysis

3.5.1. One-way ANOVA:

A one-way analysis of variance was performed in this study using SPSS software to ascertain the contribution of HMs and PAHs in several environmental matrices, including coal, CFA, and BA, as indicated in Table 3. As, Cd, Co, Cr, Hg, and Zn were found to have statistically significant differences (Table 3) among coal, CFA and BA matrices, whereas significant differences (Table 3) between PAHs from coal, CFA, and BA matrices were identified for Naphthalene, Acenaphthylene, Fluorene + Acenaphthene, Phenanthrene, Fluoranthene, Pyrene, Benz(a)anthracene + Chrysene, Benz(k)fluoranthene, Benz(B) fluoranthene, Benz(a)pyrene, Dibenz(ah)anthracene, Indeno[1,2,3-cd]pyrene+ Benz(g,h,i)perylene.

3.5.2. LSD Post Hoc Tests

Least Significant Difference (LSD) refers to the statistical significance of the smallest differences in mean value. In a one-way ANOVA, the p-values indicated whether a group difference was significant or not, but they did not compare one group to another, such as the significance between groups 1 and 2, 2 and 3, and 1 and 3, respectively. LSD Multiple comparisons are one way that the ANOVA does not account for this. The LSD Post Hoc Test has compared the concentration of HMs and PAHs in environmental matrices, such as coal, CFA and BA. Table 4 contains the pairwise comparisons. All of the examined groups had p-values under 0.05, indicating significant differences across all comparisons. The transfer behaviour of HMs of coal to CFAC is found significant for As, Cd, Co, Cr, Hg, Ni, Pb, Se, and Zn, whereas the transfer behaviour of HMs of coal to BA is significant for Co, Cr, Pb, and Zn. The transfer behaviour of PAHs of coal to CFA is found significant for Naphthalene, Acenaphthylene, Phenanthrene, Fluoranthene, Pyrene, Benz(a)anthracene + Chrysene, Benz(k)fluorenthene, Benz(b)fluoranthene, Benz(a)pyrene, Dibenz(a,h)anthracene, Indeno(1,2,3-cd)pyrene + Benz(g,h,i)perylene, while the transfer behaviour of PAHs of coal to BA is significant for Naphthalene, Acenaphthylene, Fluorene + Acenaphthene, Phenanthrene, Fluoranthene, Pyrene, Benz(a)anthracene+Chrysene, Benz(k) fluoranthene, Benz(b)fluoranthene, Dibenzo(a,h)anthracene, Indeno(1,2,3-c,d)pyrene+Benz(g,h,i) perylene (Table 5).

Table 3: The demonstration of the One-Way ANOVA test among HMs and PAHs of coal, coal fly ash, and bottom ash

Sl. No.	Between Groups Sum of Squares (coal, fly ash, and bottom ash)	df	Mean	Square	F	Sig. Value
1	As	18.86	2	9.43*	21.81	0.002
2	Cd	8.4	2	4.20*	11.98	0.008
3	Co	838.45	2	419.25*	11.71	0.008
4	Cr	5008.72	2	2504.36*	10.34	0.011
5	Cu	165.11	2	82.56	0.19	0.835
6	Hg	0.66	2	0.33*	5.26	0.048
7	Ni	1216.61	2	608.31	3.61	0.094
8	Pb	20719.59	2	10359.79	4.66	0.060
9	Se	0.28	2	0.14	4.43	0.066
10	Zn	10812.59	2	5406.30*	12.3	0.008
11	Naphthalene	54.29	2	27.14*	806.28	0.000
12	Acenaphthylene	20.44	2	10.22*	127.31	0.000
13	Fluorene + Acenaphthene	1021.46	2	510.73*	9.97	0.012
14	Phenanthrene	8.61	2	4.30*	1600.24	0.000
15	Anthracene	0.01	2	0.002	2.35	0.177
16	Fluoranthene	7.47	2	3.74*	365.97	0.000
17	Pyrene	8.76	2	4.38*	83.94	0.000
18	Benz(a)anthracene + Chrysene	11.17	2	5.59*	325.95	0.000

Cite: P. Kumar et al., "Qualitative and Quantitative Analyses of Hazardous Compounds from NTPC Rihand, India". Evergreen, 12 (03) 1402-1417 (2025). https://doi.org/10.5109/7388837.

19	Benz(k)fluorenthene	95.94	2	47.97*	3309.29	0.000
20	Benz(B)fluorenthene	12.93	2	6.47*	225.56	0.000
21	Benz(a)pyrene	0.01	2	0.003*	9.78	0.013
22	Dibenz(ah)anthracene	1.1	2	0.55*	14.94	0.005
23	Indeno(123cd)pyrene + Benz(ghi)perylene	95.1	2	47.55	1833.95	0.000*

* The mean difference is significant at 0.05 level.

3.5.3. Pearson correlation analysis

To determine the relationship between HMs and PAHs in coal, CFA, and BA, a two-tailed bivariate correlation was done by Pearson correlation methods in SPSS. For coal, CFA and BA, statistical correlation analysis was conducted in this study at the 0.05 and 0.01 levels, and the results are shown in Tables 6, 7, and 8. The association of As with Benz(k)fluoranthene in coal and Se in BA was found to be significant at the 0.05 level. The correlation was observed to be significant with Cd at 0.05 level with Pyrene and significant at 0.01 level with Hg in coal, significant at 0.05 level with Ni, Fluoranthene, Benz(a)anthracene +Chrysene in CFA, significant at 0.05 level with Ni, and significant at 0.01 level with Benz(a)anthracene + Chrysene in BA. The correlation was shown to be significant for Co at a level of 0.05 with Cr and Zn, significant at a level of 0.01 with Anthracene in coal, significant at a level of 0.05 with Anthracene in CFA, and significant at a level of 0.05 with Fluoranthene and Benz(k)fluoranthene in BA. After analysis, it was determined that the association was significant for Cr at the 0.01 level with anthracene and fluoranthene in coal and significant at the 0.01 level with

Cu and Ni in BA. Only with Ni in the BA was the link with Cu with the 0.01 threshold considered to be meaningful. Only with Cd in coal was the connection with Hg found to be significant at the 0.01 level. The connection was determined to be significant with Pb at 0.05 level with Indeno[1,2,3-cd] pyrene + Benz(g,h,i)perylene in BA and significant at 0.01 level with Fluorene + Acenaphthene and Benz(a)anthracene + Chrysene in CFA. Se was found to significantly influence the association between Naphthalene and Benz(B)fluoranthene in coal at the 0.01 level, Anthracene in CFA at the 0.05 level, and As in BA at the 0.05 level. The correlation was found to be significant with Zn at 0.05 level with Co and Anthracene in coal, significant at 0.05 level with Anthracene in CFA. Phenanthrene and acenaphthylene were found to correlate significantly at the 0.01 level in the BA. The connection of Fluorene + Acenaphthene was shown to be significant with Pb in coal and Benz(a)anthracene + Chrysene in CFA at a level of 0.01 and 0.05, respectively.

Table 4: LSD post hoc test for HMs in coal, coal fly ash, and bottom ash being demonstrated

Parameter	(I)	Environmental Matrix	Mean Difference (I-J)	Std.Error	Sig.
As	Coal	Fly Ash	-3.07033*	0.53699	0.001
		Bottom Ash	0.00200	0.53699	0.997
Cd	Coal	Fly Ash	-2.35900*	0.48375	0.003
		Bottom Ash	-1.00367	0.48375	0.083
Co	Coal	Fly Ash	-23.50167*	4.88557	0.003
		Bottom Ash	-13.98767*	4.88557	0.029
Cr	Coal	Fly Ash	-51.09533*	12.70923	0.007
		Bottom Ash	-48.92100*	12.70923	0.008
Cu	Coal	Fly Ash	-0.46067	17.18313	0.979
		Bottom Ash	8.84700	17.18313	0.625
Hg	Coal	Fly Ash	-0.65033*	0.20502	0.019
		Bottom Ash	-0.44667	0.20502	0.072
Ni	Coal	Fly Ash	-27.53467*	10.60480	0.041
		Bottom Ash	-20.06733	10.60480	0.107
Pb	Coal	Fly Ash	-111.27967*	38.51792	0.028
		Bottom Ash	-88.38767	38.51792	0.062
Se	Coal	Fly Ash	-0.41033*	0.14634	0.031
		Bottom Ash	-0.07867	0.14634	0.61
Zn	Coal	Fly Ash	-84.16367*	17.11887	0.003
		Bottom Ash	-51.75933*	17.11887	0.023

*. The mean difference is significant at the 0.05 level.

Table 5: The revelation of LSD post hoc test among PAHs of coal, coal fly ash, and bottom ash

Sl. No.	Parameter	(I)	Environmental Matrix	Mean Difference (I-J)	Sig.
1	Naphthalene	Coal	Fly Ash	5.16967*	0.000
			Bottom Ash	5.24945*	0.000
2	Acenaphthylene	Coal	Fly Ash	3.13331*	0.000
			Bottom Ash	3.25707*	0.000
3	Fluorene + Acenaphthene	Coal	Fly Ash	-0.91532	0.881
			Bottom Ash	-23.04310*	0.008
4	Phenanthrene	Coal	Fly Ash	2.04625*	0.000
			Bottom Ash	2.10230*	0.000
5	Anthracene	Coal	Fly Ash	0.03778	0.128
			Bottom Ash	-0.00434	0.846
6	Fluoranthene	Coal	Fly Ash	2.00109*	0.000
			Bottom Ash	1.85775*	0.000
7	Pyrene	Coal	Fly Ash	2.19091*	0.000
			Bottom Ash	1.97984*	0.000
8	Benz(a)anthracene + Chrysene	Coal	Fly Ash	2.34876*	0.000
			Bottom Ash	2.37842*	0.000
9	Benz(k)fluorenthene	Coal	Fly Ash	6.94471*	0.000
			Bottom Ash	6.90780*	0.000
10	Benz(B)fluorenthene	Coal	Fly Ash	2.54325*	0.000
			Bottom Ash	2.54325*	0.000
11	Benz(a)pyrene	Coal	Fly Ash	-0.06067*	0.006
			Bottom Ash	-0.01141	0.464
12	Dibenz(ah)anthracene	Coal	Fly Ash	0.71003*	0.004
			Bottom Ash	0.77050*	0.003
13	Indeno(123cd)pyrene + Benz(ghi)perylene	Coal	Fly Ash	7.06768*	0.000
			Bottom Ash	6.70988*	0.000

* The mean difference is significant at the 0.05 level.

Table 6: Pearson correlation analysis among PAHs and HMs in coal samples

S.N.	HMS & PAHs	1	2	3	4	5	6	7	8	9	10	11	12	13	14	15	16	17	18	19	20	21	22	23
1	As	1																						
2	Cd	-0.10	1																					
3	Co	0.90	0.34	1																				
4	Cr	-0.93	-0.28	-.998*	1																			
5	Cu	-0.72	-0.61	-0.95	0.93	1																		
6	Hg	-0.11	1.0**	0.33	-0.27	-0.60	1																	
7	Ni	0.94	-0.44	0.69	-0.74	-0.44	-0.45	1																
8	Pb	-0.45	-0.84	-0.79	0.75	0.94	-0.84	-0.11	1															
9	Se	-0.37	0.96	0.07	-0.01	-0.37	0.96	-0.67	-0.67	1														
10	Zn	-0.88	-0.38	-.999*	0.99	0.96	-0.37	-0.66	0.82	-0.11	1													
11	Naphthalene	0.37	-0.96	-0.07	0.00	0.37	-0.96	0.67	0.66	-1.0**	0.11	1												
12	Acenaphthylene	-0.96	0.37	-0.75	0.79	0.51	0.38	-1.00	0.19	0.61	0.72	-0.61	1											
13	Fluorene+Acenaphthene	-0.47	-0.83	-0.81	0.77	0.95	-0.82	-0.13	1.000*	-0.65	0.83	0.64	0.21	1										
14	Phenanthrene	0.60	-0.86	0.19	-0.26	0.11	-0.86	0.84	0.45	-0.96	-0.15	0.97	-0.80	0.42	1									
15	Anthracene	0.90	0.35	1.0**	-.99*	-0.95	0.34	0.69	-0.80	0.08	-.99*	-0.07	-0.74	-0.81	0.19	1								
16	Fluoranthene	-0.95	-0.22	-0.99	.998*	0.91	-0.21	-0.78	0.71	0.06	0.99	-0.06	0.83	0.73	-0.32	-0.99	1							
17	Pyrene	-0.03	.997*	0.41	-0.35	-0.67	1.00	-0.37	-0.88	0.94	-0.45	-0.94	0.30	-0.87	-0.81	0.42	-0.29	1						
18	Benz(a)anthracene+ Chrysene	-0.46	-0.84	-0.80	0.76	0.95	-0.83	-0.12	1.0**	-0.65	0.83	0.65	0.20	1. 0**	0.43	-0.81	0.72	-0.88	1					
19	Benz(k)fluorenthene		-.998*	0.16	-0.87	0.90	0.68	0.17	-0.96	0.39	0.42	0.85	-0.43	0.98	0.42	-0.65	-0.87	0.93	0.08	0.41	1			
20	Benz(B)fluorenthene	0.35	-0.97	-0.09	0.03	0.39	-0.97	0.66	0.68	-1.0*	0.13	1.0*	-0.60	0.66	0.96	-0.10	-0.04	-0.94	0.67	-0.41	1			
21	Benz(a)pyrene	-0.81	-0.50	-0.98	0.97	0.99	-0.49	-0.56	0.89	-0.24	0.99	0.24	0.62	0.90	-0.02	-0.99	0.95	-0.56	0.89	0.78	0.26	1		
22	Dibenz(ah)anthracene	0.98	-0.29	0.80	-0.84	-0.58	-0.30	0.99	-0.27	-0.54	-0.77	0.55	-1.00	-0.29	0.74	0.80	-0.87	-0.22	-0.28	-0.99	0.53	-0.68	1	
23	Indeno(123cd)pyrene+ Benz(ghi)perylene	0.29	-0.98	-0.15	0.09	0.45	-0.98	0.61	0.72	-1.00	0.19	1.00	-0.54	0.71	0.94	-0.16	0.03	-0.96	0.71	-0.35	.998*	0.32	0.47	1

**. Correlation is significant at the 0.05 level (2-tailed), **. Correlation is significant at the 0.01 level (2-tailed).*

Cite: P. Kumar et al., "Qualitative and Quantitative Analyses of Hazardous Compounds from NTPC Rihand, India". Evergreen, 12 (03) 1402-1417 (2025). https://doi.org/10.5109/7388837.

Table 7: Pearson correlation analysis among PAHs and HMs in fly ash samples

S.N.	PAHs and HMs	1	2	3	4	5	6	7	8	9	10	11	12	13	14	15	16	17	18	19	20	21	22	23	
1	As		1																						
2	Cd		0.55	1																					
3	Co		-0.94	-0.80	1																				
4	Cr		-0.80	0.06	0.55	1																			
5	Cu		-0.82	-0.93	0.97	0.32	1																		
6	Hg		0.64	-0.29	-0.34	-0.97	-0.09	1																	
7	Ni		0.51	.999*	-0.77	0.11	-0.91	-0.34	1																
8	Pb		-0.99	-0.66	0.98	0.71	0.89	-0.52	-0.63	1															
9	Se		0.97	0.74	-1.00	-0.63	-0.94	0.43	0.71	-0.99	1														
10	Zn		0.99	0.65	-0.98	-0.72	-0.89	0.53	0.62	-1.0**	0.99	1													
11	Naphthalene		-0.20	0.71	-0.15	0.74	-0.40	-0.88	0.74	0.06	0.05	-0.07	1												
12	Acenaphthylene		-0.57	0.38	0.25	0.95	-0.01	-1.00	0.43	0.44	-0.34	-0.45	0.92	1											
13	Fluorene+Acenaphthene		0.72	0.97	-0.91	-0.17	-0.99	-0.07	0.96	-0.81	0.87	0.81	0.53	0.16	1										
14	Phenanthrene		0.45	0.99	-0.73	0.17	-0.88	-0.39	.998*	-0.58	0.66	0.57	0.78	0.48	0.94	1									
15	Anthracene		-0.95	-0.77	.999*	0.58	0.96	-0.38	-0.74	0.99	-.999*	-0.98	-0.11	0.29	-0.90	-0.70	1								
16	Fluoranthene		0.59	.999*	-0.83	0.01	-0.95	-0.24	0.99	-0.70	0.78	0.69	0.67	0.33	0.98	0.99	-0.81	1							
17	Pyrene		-0.94	-0.24	0.78	0.95	0.59	-0.86	-0.20	0.89	-0.83	-0.89	0.51	0.80	-0.46	-0.14	0.80	-0.29	1						
18	Benz(a)anthracene+Chrysene		-0.58	-.999*	0.82	-0.02	0.94	0.25	-1.00	0.69	-0.77	-0.69	-0.68	-0.34	-0.98	-0.99	0.80	-1.0**	0.28	1					
19	Benz(k)fluorenthene		-0.70	-0.98	0.90	0.14	0.98	0.10	-0.97	0.80	-0.86	-0.79	-0.56	-0.19	-1.0*	-0.95	0.89	-0.99	0.43	0.99	1				
20	Benz(B)fluorenthene		.a	.a	.a	.a	.a	.a	.a	.a	.a	.a	.a	.a	.a	.a	.a	.a	.a	.a	.a	.a			
21	Benz(a)pyrene		0.33	0.97	-0.63	0.29	-0.81	-0.51	0.98	-0.47	0.56	0.46	0.86	0.59	0.89	0.99	-0.60	0.96	-0.01	-0.96	-0.91	.a	1		
22	Dibenz(ah)anthracene		0.74	-0.16	-0.47	-0.99	-0.22	0.99	-0.21	-0.63	0.54	0.64	-0.81	-0.97	0.07	-0.27	-0.50	-0.11	-0.92	0.12	-0.04	.a	-0.39	1	
23	Indeno(123cd)pyrene+ Benz(ghi)perylene		0.99	0.40	-0.87	-0.89	-0.71	0.76	0.35	-0.95	0.91	0.95	-0.36	-0.70	0.60	0.30	-0.89	0.45	-0.99	-0.44	-0.57	.a	0.17	0.84	1

**. Correlation is significant at the 0.05 level (2-tailed), **. Correlation is significant at the 0.01 level (2-tailed). a. Cannot be computed because at least one of the variables is constant.*

Table 8: Pearson correlation analysis among PAHs and HMs in bottom ash samples.

S.N.	PAHs and HMs	1	2	3	4	5	6	7	8	9	10	11	12	13	14	15	16	17	18	19	20	21	22	23
1	As	1																						
2	Cd	-0.05	1																					
3	Co	0.44	0.87	1																				
4	Cr	0.03	1.00	0.91	1																			
5	Cu	0.03	1.00	0.91	1.0**	1																		
6	Hg	-0.97	-0.19	-0.64	-0.26	-0.27	1																	
7	Ni	0.01	.998*	0.90	1.0*	1.0*	-0.25	1																
8	Pb	-0.49	0.90	0.57	0.86	0.86	0.27	0.87	1															
9	Se	.999*	-0.01	0.48	0.07	0.07	-0.98	0.05	-0.45	1														
10	Zn	-0.19	0.99	0.80	0.98	0.98	-0.05	0.98	0.95	-0.15	1													
11	Naphthalene	0.93	-0.41	0.09	-0.33	-0.33	-0.82	-0.35	-0.77	0.92	-0.53	1												
12	Acenaphthylene	0.77	-0.67	-0.23	-0.61	-0.61	-0.60	-0.62	-0.93	0.75	-0.77	0.95	1											
13	Fluorene+Acenaphthene	0.62	-0.81	-0.43	-0.77	-0.76	-0.42	-0.78	-0.99	0.59	-0.89	0.86	0.98	1										
14	Phenanthrene	-0.78	0.67	0.22	0.61	0.61	0.61	0.62	0.93	-0.75	0.77	-0.95	-1.0**	-0.98	1									
15	Anthracene	-0.82	-0.53	-0.88	-0.60	-0.60	0.93	-0.59	-0.11	-0.84	-0.41	-0.55	-0.27	-0.06	0.27	1								
16	Fluoranthene	0.39	0.90	.998*	0.93	0.93	-0.59	0.93	0.62	0.42	0.83	0.03	-0.29	-0.48	0.28	-0.85	1							
17	Pyrene	-0.57	-0.79	-0.99	-0.84	-0.84	0.74	-0.83	-0.45	-0.60	-0.70	-0.23	0.08	0.29	-0.08	0.94	-0.98	1						
18	Benz(a)anthracene+Chrysene	0.06	-1.0**	-0.87	-1.00	-1.00	0.17	-.997*	-0.90	0.02	-0.99	0.42	0.68	0.82	-0.68	0.52	-0.90	0.79	1					
19	Benz(k)fluorenthene	0.49	0.85	.999*	0.89	0.89	-0.68	0.88	0.53	0.52	0.76	0.14	-0.18	-0.38	0.17	-0.90	0.99	-1.00	-0.84	1				
20	Benz(B)fluorenthene	.b	.b	.b	.b	.b	.b	.b	.b	.b	.b	.b	.b	.b	.b	.b	.b	.b	.b	.b	.b			
21	Benz(a)pyrene	0.87	0.46	0.83	0.52	0.53	-0.96	0.51	0.02	0.89	0.33	0.63	0.35	0.15	-0.36	-1.00	0.80	-0.90	-0.44	0.86	.b	1		
22	Dibenz(ah)anthracene	.b	.b	.b	.b	.b	.b	.b	.b	.b	.b	.b	.b	.b	.b	.b	.b	.b	.b	.b	.b	.b	.b	
23	Indeno(123cd)pyrene+ Benz(ghi)perylene	0.54	-0.87	-0.52	-0.83	-0.83	-0.32	-0.84	-.998*	0.50	-0.93	0.80	0.95	0.99	-0.95	0.05	-0.57	0.39	0.88	-0.48	.b	0.04	.b	1

**. Correlation is significant at the 0.05 level (2-tailed), **. Correlation is significant at the 0.01 level (2-tailed). b. Cannot be computed because at least one of the variables is constant.*

The calculated association between phenanthrene and acenaphthylene in BA was significant at the 0.01 level. The correlation with anthracene was shown to be significant at a level of 0.05 with Zn and Cr, at a level of 0.01 with Co in coal, and at a level of 0.05 with Se in CFA. The association was shown to be significant for fluoranthene with Cr in coal at 0.05 level, significant for Cd at 0.05 level, significant for Benz(a)anthracene + Chrysene in CFA at 0.01 level, and significant for Co in BA at 0.05 level. At the 0.05 level, it was determined that the association between Pyrene and Cd in coal was significant. The correlation was found to be significantly correlated with Benz(a)anthracene + Chrysene at 0.01 level with Pb and Fluorene+ Acenaphthene in Coal, significantly correlated at 0.05 level with Cd, and significantly correlated at 0.01 level with Fluoranthene in CFA, and significantly correlated at 0.01 level with Cd and significantly correlated at 0.05 level with Ni in BA. The connection was determined to be significant for Benz(k)fluoranthene with As in coal at 0.05 level, significant for Fluorene + Acenaphthene in CFA at 0.01 level, and significant for Co in BA at 0.05 level. The association between Benz(b)fluoranthene, Naphthalene, and Se in coal was shown to be significant at the 0.01 level. The link was found to be significant with Indeno(1,2,3-c,d) pyrene + Benz(g,h,i)perylene at 0.05 level with Benz(b)fluorenthene in coal and significant at 0.05 level with Pb in BA.

3.5.4. Hierarchical Cluster Analysis

Hierarchical cluster analysis (HCA) is a sophisticated and useful way that grouped together all objects according to how similar they are. A metric that provides a visually appealing dendrogram and separates/clusters the groups was used to perform HCA: ward linkage with rescaling distance cluster combined as similarity. Figure 2, 3, and 4 for both seasons of the HCA classify HMs and PAHs in coal, CFA and BA. In coal, HMs and PAHs are grouped into two major classes, which are then sequentially subdivided into two subgroups. Cluster 1 in coal is made up of the following compounds: Se, Anthracene, Benz(a)pyrene, Hg, Cd, As, Dibenz(a,h)anthracene, Benz(a)anthracene + Chrysene, Benz(B)fluoranthene, and Phenanthrene. Cluster 2 was represented by the compounds Pyrene, Fluoranthene, Acenaphthylene, Benz(k)fluoranthene, Indeno(1,2,3-c,d) pyrene + Benz(g,h,i)perylene, Co, and Naphthalene. Cluster 3 was produced by Cr, Fluorene + Acenaphthene, Zn, and Ni, whereas Cu and Pb were divided into clusters 4 and 5 (Figure 5). In CFA, HMs, and PAHs are grouped into two major classes, which are further divided into two subgroups. Cluster 1 formed with Anthracene, Benz(B)fluoranthene, Dibenzo(a,h)anthracene, Indeno(1,2,3-c,d)pyrene + Benz(g,h,i)perylene Pyrene, Benzo(a)anthracene + Chrysene, Fluoranthene, Benz(a)pyrene, Phenanthrene, Benz(k)fluoranthene, Acenaphthylene. Se, Naphthalene, Hg, As, and Cd, represent cluster 2. Cu, Fluorene + Acenaphthene, Co, and Ni were developed into cluster 3, whereas Cr and Zn were separated into cluster 4 and Pb into cluster 5. Benz(B)fluoranthene, Dibenzo(ah)anthracene, Phenanthrene, Benz(a)pyrene, Anthracene, Benz(a)anthracene + Chrysene, Fluoranthene, Benz(k)fluorenthene, Se, Acenaphthylene and Naphthalene are grouped into cluster 1, Indeno(1,2,3-c,d)pyrene + Benz(g,h,i)perylene, As, Hg, Pyrene, and Cd were represented to cluster 2, Cr and Zn formed to cluster 3, Co and Cu was separated into cluster 4 while Fluorene + Acenaphthene and Pb was separated into cluster 5 in BA sample.

4. Conclusion

The present study has determined that selected coal-fired power plant samples namely coal, CFA, and BA, exhibited adequate concentrations of HMs and PAHs. Ten distinct HMs were evaluated by quantification using an appropriate methodology, revealing the presence of varying concentrations of ∑16 PAHs in the processed samples. The increasing trends of heavy metals in coal, CFA and BA were determined Se<Hg<Cd<As<Co<Ni<Zn<Cr<Cu<Pb, Se<Hg<Cd<As<Co<Cu<Ni<Cr<Zn<Pb, and Se<As<Hg<Cd<Co<Cu<Ni<Zn<Cr<Pb, respectively. HCA is an advanced and effective method for categorizing data into clusters of similar entities, typically organized into five groups. The results of one-way ANOVA showed a significant difference found in 6 HMs of 13 PAHs of the coal, CFA, and BA samples. The correlation is found significant for Co with Cr and Zn at 0.05 level and
Cd with Hg at 0.01 level among HMs in coal for Ni with Cd at 0.05 level and Zn with Pb at 0.01 level among HMs in CFA, and for Se with As at 0.05 level and Cu with Ni at 0.01 level among HMs in BA. If the emissions from spotted coal-fired power plants reach into succeeding atmospheres, they may contaminate the soil, water, and air quality. The relatively high concentration of HMs that was discovered in the CFA sample suggested that it was enriched with HMs and that they may be emitted when the coal is burned. Pollution caused by related pollutants may pose risks to both human health and the environment and can have a wide range of toxicological effects. Effective measures might need to be taken to mitigate the hazards associated with power plants, such as the adoption of advanced pollution control technology, enhancing the efficiency of coal-fired power plants, and switching to renewable energy sources. Likewise, incentivizing energy-efficient initiatives and promoting energy-conserving behavior can effectively mitigate energy demand and lessen dependence on coal-based power generation facilities.

Cite: P. Kumar et al., "Qualitative and Quantitative Analyses of Hazardous Compounds from NTPC Rihand, India". Evergreen, 12 (03) 1402-1417 (2025). https://doi.org/10.5109/7388837.

Acknowledgements

Author PK expresses gratitude to the University Grants Commission (UGC), New Delhi, India, for the financial support provided for Ph.D. research, as well as to the Academy of Scientific & Innovative Research (AcSIR), *an Institute of National Importance*.

Conflict of interest

No conflict of interest existed, as declared by the authors.

References

1) U. Kleinhans, C. Wieland, F.J. Frandsen, and H. Spliethoff, "Ash formation and deposition in coal and biomass fired combustion systems: progress and challenges in the field of ash particle sticking and rebound behavior," Prog. Energy Combust. Sci., 68 65–168 (2018). doi:10.1016/j.pecs.2018.02.001.
2) Central Electricity Authority, "Flyash generation at coal/lignite based thermal power stations and its utilization in the country," 2019.
3) B.J. Mathew, M. Sudhakar, and C. Natarajan, "Strength , economic and sustainability characteristics of coal ash – ggbs based geopolymer concrete .," Int. J. Comput. Eng. Res., 3 (1) 207–212 (2013).
4) A. Karthik, K. Sudalaimani, and C.T. Vijayakumar, "Durability study on coal fly ash-blast furnace slag geopolymer concretes with bio-additives," Ceram. Int., 43 (15) 11935–11943 (2017). doi:10.1016/j.ceramint.2017.06.042.
5) X. Querol, F. Plana, A. Alastuey, N. Moreno, M. Izquierdo, O. Font, T. Moreno, S. Diez, and M. Barra, "Environmental, physical and structural characterisation of geopolymer matrixes synthesised from coal (co-) combustion fly ashes," J. Hazard. Mater., 154 (2008) 175–183 (2008). doi:10.1016/j.jhazmat.2007.10.008.
6) ASTMC 618 19, "Standard Specification for Coal Fly Ash and Raw or Calcined Natural Pozzolan for Use in concrete," 2019. doi:10.1520/C0618-19.2.
7) R. Cai, H. Zhang, M. Zhang, H. Yang, J. Lyu, and G. Yue, "Development and application of the design principle of fluidization state specification in cfb coal combustion," Fuel Process. Technol., 174 (August 2017) 41–52 (2018). doi:10.1016/j.fuproc.2018.02.009.
8) L. Del Zotto, A. Tallini, G. Di Simone, G. Molinari, and L. Cedola, "Energy enhancement of solid recovered fuel within systems of conventional thermal power generation," Energy Procedia, 81 319–338 (2015). doi:10.1016/j.egypro.2015.12.102.
9) A. Demirbas, "Combustion characteristics of different biomass fuels," Prog. Energy Combust. Sci., 30 (2) 219–230 (2004). doi:10.1016/j.pecs.2003.10.004.
10) S. Ciukaj, and B. Hernik, "Field and cfd study of fuel distribution in pulverized fuel (pf) boilers," J. Therm. Sci., 29 (3) 535–545 (2020). doi:10.1007/s11630-020-1199-0.
11) K.A. Komnitsas, "Procedia engineering potential of geopolymer technology towards green buildings and sustainable cities," Procedia Eng., (2011). doi:10.1016/j.proeng.2011.11.2108.
12) D. Or, and T.A. Ghezzehei, "Modeling post-tillage soil structural dynamics: a review," Soil Tillage Res., 64 (1–2) 41–59 (2002). doi:10.1016/S0167-1987(01)00256-2.
13) X.Y. Zhuang, L. Chen, S. Komarneni, C.H. Zhou, D.S. Tong, H.M. Yang, W.H. Yu, and H. Wang, "Fly ash-based geopolymer: clean production, properties and applications," J. Clean. Prod., 125 253–267 (2016). doi:10.1016/j.jclepro.2016.03.019.
14) ASTMC1585 20, "Standard test method for measurement of rate of absorption of water by hydraulic cement concretes," ASTM Int., 41 (147) 1–6 (2013). doi:10.1520/C1585-20.2.
15) S.A. Ishak, and H. Hashim, "Low carbon measures for cement plant - a review," J. Clean. Prod., 103 260–274 (2015). doi:10.1016/j.jclepro.2014.11.003.
16) P. Chindaprasirt, P. De Silva, K. Sagoe-Crentsil, and S. Hanjitsuwan, "Effect of sio2and al2o3on the setting and hardening of high calcium fly ash-based geopolymer systems," J. Mater. Sci., (2012). doi:10.1007/s10853-012-6353-y.
17) H.P. Nielsen, F.J. Frandsen, K. Dam-Johansen, and L.L. Baxter, "Implications of chlorine-associated corrosion on the operation of biomass-fired boilers," Prog. Energy Combust. Sci., 26 (3) 283–298 (2000). doi:10.1016/S0360-1285(00)00003-4.
18) G. Roviello, L. Ricciotti, A.J. Molino, C. Menna, C. Ferone, D. Asprone, R. Cioffi, V. Ferrandiz-Mas, P. Russo, and O. Tarallo, "Hybrid fly ash-based geopolymeric foams: microstructural, thermal and mechanical properties," Materials (Basel)., 13 (13) 1–19 (2020). doi:10.3390/ma13132919.
19) Y.D.T. Cheng; Yu-sheng Dai, "Application of geopolymer paste for concrete repair," Struct. Concr., (May 2018) 1–11 (2017). doi:10.1002/suco.201600161.
20) S.M. Mustakim, S.K. Das, J. Mishra, A. Aftab, T.S. Alomayri, H.S. Assaedi, and C.R. Kaze, "Improvement in fresh, mechanical and microstructural properties of fly ash- blast furnace slag based geopolymer concrete by addition of nano and micro silica," Silicon, 13 (2021) 2415–2428 (2020). doi:10.1007/s12633-020-00593-0.
21) M. Safiuddin, M.A. Salam, and M.Z. Jumaat, "Key

fresh properties of self-consolidating high-strength pofa concrete," J. Mater. Civ. Eng., 26 (1) 134–142 (2014). doi:10.1061/(asce)mt.1943-5533.0000782.

22) J. Chen, T. Ma, Y. Lu, J. Wang, M. Zhang, L. Lin, C. Yan, X. Li, and H. Chen, "Improved technology for rounding graphite: machine structure and industrial test," Appl. Sci., 13 (17) (2023). doi:10.3390/app13179820.
23) F. Matalkah, P. Soroushian, A. Balchandra, and A. Peyvandi, "Characterization of alkali-activated nonwood biomass ash – based geopolymer concrete," J. Mater. Civ. Eng., 29 (4) 1–9 (2017). doi:10.1061/(ASCE)MT.1943-5533.
24) U. Sharma, N. Gupta, A. Bahrami, Y.O. Özkılıç, and M. Verma, "Behavior of fibers in geopolymer concrete : a comprehensive review," Buildings, 14 (136) 1–28 (2024). doi:https://doi.org/10.3390/buildings14010136.
25) Y.H.M. Amran, R. Alyousef, H. Alabduljabbar, and M. El-Zeadani, "Clean production and properties of geopolymer concrete; a review," J. Clean. Prod., 251 119679 (2020). doi:10.1016/j.jclepro.2019.119679.
26) J. Kang, C. Xie, Q. Peng, N. Wang, X. Wang, and Y. Zhang, "Analysis of feed inlet and optimal feeding amount of waste ground film impurity removal equipment," Appl. Sci., 13 (17) (2023). doi:10.3390/app13179905.
27) H. Sethi, P.P. Bansal, and R. Sharma, "Effect of addition of ggbs and glass powder on the properties of geopolymer concrete," Iran. J. Sci. Technol. - Trans. Civ. Eng., 43 (4) 607–617 (2019). doi:10.1007/s40996-018-0202-4.
28) B.R. Sathi, S.N. Gurugubelli, and H.B. N, "The effect of ecap on structural morphology and wear behaviour of 5083 al composite reinforced with red mud," Evergr. Jt. J. Nov. Carbon Resour. Sci. Green Asia Strateg., 10 (02) 774–781 (2023).
29) M. Awi, and A.S. Abdullah, "A review on mechanical properties and response of fibre metal laminate under impact loading (experiment)," Evergreen, 10 (1) 111–129 (2023). doi:10.5109/6781057.
30) M. Sharma, N.L. Jain, and J.K. Purohit, "Analysis of circular economy enablers in manufacturing context for indian industries: a electre method ranking process," Evergreen, 10 (3) 1156–1168 (2023). doi:10.5109/7148437.
31) S. Nayak, and M.P. Kumar, "Mechanical characterization and static analysis of natural fiber based composite propeller blade mechanical characterization and static analysis of natural fiber based composite propeller blade," Evergr. Jt. J. Nov. Carbon Resour. Sci. Green Asia Strateg., 10 (2) 805–812 (2023).
32) G.G. Goswami, R. Sarwar, M. Rahman, D.C. Panday, I.J. Ishita, T. Labib, and N.V. Motiram, "Why did india pull out of regional comprehensive economic partnership (rcep)? a gravity explanation of the indian puzzle," Environ. Dev. Sustain., 10 (03) 1140–1155 (2023).
33) A. Chaudhary, "Road surface quality detection using light weight neural network for visually impaired pedestrian road surface quality detection using light weight neural," Evergr. Jt. J. Nov. Carbon Resour. Sci. Green Asia Strateg., 10 (2) 706–714 (2023).
34) N.K. Yadav, N.S. Rajput, S. Kulshreshtha, and M.K. Gupta, "Investigation of the mechanical and wear properties of epoxy resin composite (ercs) made with nano particle tio2 and cotton fiber reinforcement," Evergreen, 10 (1) 63–77 (2023). doi:10.5109/6781041.
35) R. Kumar, M. Verma, and N. Dev, "Analysis of pce-based superplasticiser for the different types of cement using marsh cone test," Evergreen, 11 (2) 665–672 (2024). doi:10.5109/7183337.
36) R. Kumar, N. Dev, S. Ram, and M. Verma, "Investigation of dry-wet cycles effect on the durability of modified rubberised concrete," Forces Mech., 10 (2023) 100168 (2023). doi:10.1016/j.finmec.2023.100168.
37) N. Kumar, R.D. Raut, K. Upreti, M.S. Alam, M. Shafiuddin, and M. Verma, "Environmental Concern in TPB Model for Sustainable IT Adoption," in: Int. Conf. Inf. Syst. Intell. Appl. Lect. Notes Networks Syst. 550, 2023: pp. 59–70. doi:10.1007/978-3-031-16865-9_5.
38) R. Kumar, M. Verma, and N. Dev, "Investigation on the effect of seawater condition, sulphate attack, acid attack, freeze–thaw condition, and wetting–drying on the geopolymer concrete," Iran. J. Sci. Technol. Trans. Civ. Eng. Civ. Eng., 46 (4) 2823–2853 (2022). doi:10.1007/s40996-021-00767-9.
39) U. Sharma, N. Gupta, and M. Verma, "Prediction of compressive strength of ggbfs and flyash-based geopolymer composite by linear regression, lasso regression, and ridge regression," Asian J. Civ. Eng., 24 (8) 3399–3411 (2023). doi:10.1007/s42107-023-00721-2.
40) U. Sharma, N. Gupta, and M. Verma, "Prediction of compressive strength of geopolymer concrete using artificial neural network," Asian J. Civ. Eng., 24 (8) 2837–2850 (2023). doi:10.1007/s42107-023-00678-2.
41) K. Upreti, and M. Verma, "Prediction of compressive strength of high-volume fly ash concrete using artificial neural network," J. Eng. Res. Appl., 1 (2) 24–32 (2022). doi:10.55953/JERA.2022.2104.
42) K. Upreti, M. Verma, M. Agrawal, J. Garg, R. Kaushik, C. Agrawal, D. Singh, and R. Narayanasamy, "Prediction of mechanical strength

by using an artificial neural network and random forest algorithm," J. Nanomater., 2022 1–12 (2022). doi:DOI: 10.1155/2022/7791582.